Cellular/Molecular

The Calcium Channel $\alpha_2\delta$-2 Subunit Partitions with $Ca_V2.1$ into Lipid Rafts in Cerebellum: Implications for Localization and Function

Anthony Davies,[1]* Leon Douglas,[1]* Jan Hendrich,[1]* Jack Wratten,[1] Alexandra Tran Van Minh,[1] Isabelle Foucault,[1] Dietlind Koch,[1] Wendy S. Pratt,[1] Helen R. Saibil,[2] and Annette C. Dolphin[1]

[1]Department of Pharmacology, University College London, London WC1E 6BT, United Kingdom, and [2]School of Crystallography, Birkbeck, University of London, London WC1E 7HX, United Kingdom

The accessory $\alpha_2\delta$ subunits of voltage-gated calcium channels are highly glycosylated transmembrane proteins that interact with calcium channel $\alpha1$ subunits to enhance calcium currents. We compared the membrane localization and processing of native cerebellar $\alpha_2\delta$-2 subunits with $\alpha_2\delta$-2 stably expressed in tsA-201 cells. We identified that $\alpha_2\delta$-2 is completely concentrated in cholesterol-rich microdomains (lipid rafts) in cerebellum, in which it substantially colocalizes with the calcium channel $\alpha1$ subunit $Ca_V2.1$, although $Ca_V2.1$ is also present in the Triton X-100-soluble fraction. In tsA-201 cells, unlike cerebellum, $\alpha_2\delta$-2 is not completely proteolytically processed into α_2-2 and δ-2. However, this processing is more complete in the lipid raft fraction of tsA-201 cells, in which $\alpha_2\delta$-2 also colocalizes with $Ca_V2.1$. Cholesterol depletion of intact cells disrupted their lipid rafts and enhanced $Ca_V2.1/\alpha_2\delta$-2/$\beta4$ currents. Furthermore, $\alpha_2\delta$-2 coimmunoprecipitates with lipid raft-associated proteins of the stomatin family. The apparent affinity of $\alpha_2\delta$-2 for its ligand gabapentin is increased markedly in the cholesterol-rich microdomain fractions, in both cerebellum and the stable $\alpha_2\delta$-2 cell line. In contrast, $\alpha_2\delta$-2 containing a point mutation (R282A) has a much lower affinity for gabapentin, and this is not enhanced in the lipid raft fraction. This R282A mutant $\alpha_2\delta$-2 shows reduced functionality in terms of enhancement of $Ca_V2.1/\beta4$ calcium currents, suggesting that the integrity of the gabapentin binding site may be important for normal functioning of $\alpha_2\delta$-2. Together, these results indicate that both $\alpha_2\delta$-2 and $Ca_V2.1$ are normally associated with cholesterol-rich microdomains, and this influences their functionality.

Key words: **calcium; channel; $\alpha_2\delta$; gabapentin; lipid raft; cerebellum; cholesterol**

Introduction

Voltage-gated Ca^{2+} (Ca_V) channels are composed of a pore-forming $\alpha1$ subunit, associated, at least in the case of the Ca_V1 and 2 subfamilies, with an intracellular β subunit responsible for trafficking (Walker and De Waard, 1998) and a transmembrane $\alpha_2\delta$ subunit whose function is less well defined (Canti et al., 2003). The $\alpha1$ subunit determines the main biophysical properties of the channel and is modulated by the other subunits (Walker and De Waard, 1998). Mammalian genes encoding 10 $\alpha1$, four β, and four $\alpha_2\delta$ subunits have been identified (Catterall, 2000; Ertel et al., 2000; Burgess et al., 2001).

The topology of the $\alpha_2\delta$ protein appears to generalize for all four $\alpha_2\delta$ subunits. They are all predicted to be type 1 transmembrane proteins, because all have a hydrophobic region in the C terminus (CT) that is likely to be a transmembrane domain. All have predicted N-terminal signal sequences, indicating that the N terminus is extracellular (for review, see Canti et al., 2003). From the early studies of $\alpha_2\delta$-1 purified from skeletal and cardiac muscle, it was identified that the α_2 subunit is disulfide bonded to a transmembrane δ subunit, and both subunits are the product of a single gene, encoding the $\alpha_2\delta$ protein, which is posttranslationally cleaved into α_2 and δ (Ellis et al., 1988; De Jongh et al., 1990; Gurnett et al., 1996). The $\alpha_2\delta$-2 subunit is also clearly reduced in molecular mass by disulfide-bond reduction (Gong et al., 2001), and, when expressed heterologously, the signal sequence is cleaved and the α_2 moiety is entirely extracellular (Brodbeck et al., 2002). However, there is poor sequence conservation between $\alpha_2\delta$-1 and $\alpha_2\delta$-2 around the identified site of cleavage between α_2 and δ in $\alpha_2\delta$-1 (Jay et al., 1991).

All $\alpha_2\delta$ subunits enhance calcium currents through the high-voltage-activated (HVA) Ca_V1 and Ca_V2 channels (Gurnett et al., 1996; Klugbauer et al., 1999; Barclay et al., 2001). However, their mechanism of action remains unclear. Our recent work has shed light on this and suggests that the metal ion-dependent adhesion site (MIDAS) in the Von Willebrand factor-A (VWA) domain within $\alpha_2\delta$-2 is of key importance in trafficking $Ca_V\alpha1$ subunits (Canti et al., 2005). This VWA domain is present in all $\alpha_2\delta$ subunits and has a perfect MIDAS motif in $\alpha_2\delta$-1 and $\alpha_2\delta$-2 (Whittaker and Hynes, 2002). Both $\alpha_2\delta$-1 and $\alpha_2\delta$-2 bind the antiepileptic drugs gabapentin and pregabalin, which are also used in the

Received April 13, 2006; revised July 17, 2006; accepted July 17, 2006.

This work was supported by Medical Research Council, Biotechnology and Biological Sciences Research Council, and The Wellcome Trust. We thank K. Chaggar for technical assistance.

*A.D., L.D., and J.H. contributed equally to this work.

Correspondence should be addressed to Annette C. Dolphin, Department of Pharmacology, University College London, Gower Street, London WC1E 6BT, UK. E-mail: a.dolphin@ucl.ac.uk.

DOI:10.1523/JNEUROSCI.2764-06.2006

 0270-6474/06/268748-10$15.00/0

treatment of neuropathic pain (Brown et al., 1998; Marais et al., 2001; Canti et al., 2003).

In this study, we identified that both native and heterologously expressed $\alpha_2\delta$-2 subunits are concentrated together with $Ca_V2.1$ in Triton X-100-insoluble cholesterol-rich microdomain fractions (commonly known as lipid rafts), in which the affinity for binding [^{3}H]gabapentin is strongly enhanced and in which they interact with proteins of the stomatin family.

Materials and Methods

Molecular biology. Mouse $\alpha_2\delta$-2 [GenBank accession number AF247139; common brain splice variant, lacking exon 23 and 6 bp of exon 38 (Barclay and Rees, 2000)] was engineered with an internal hemagglutinin (HA) tag between amino acids 652 (L) and 653 (Q), using standard molecular biology techniques to form $\alpha_2\delta$-2(HA). The R282A mutation in mouse $\alpha_2\delta$-2 was made by standard techniques. All constructs were sequenced before use. Other cDNAs used were rat $Ca_V2.1$ (GenBank accession number M64373), E1686R (Hans et al., 1999), and rat β4 (LO2315), cloned into the pMT2 vector for expression in mammalian cells.

Antibodies. Ca channel antibodies (Abs) used were as follows: anti-mouse α_2-2(16–29), α_2-2(102–117) (Brodbeck et al., 2002), δ-2(1080–1094), and δ-2 CT (1133–1147) for $\alpha_2\delta$-2 (all affinity-purified rabbit anti-peptide Abs) and anti-β1b serum (Moss et al., 2002). Other primary antibodies and their sources were as follows: anti-flotillin-1 (BD Biosciences, Cowley, Oxford, UK), anti-prohibitin (Abcam, Cambridge, UK), anti-stomatin-like protein-2 (SLP-2) (BD Biosciences), anti-Akt (Cell Signaling Technology, Danvers, MA), and anti-$Ca_V2.1$ (Alomone Labs, Jerusalem, Israel).

Heterologous expression of cDNAs. Cos-7 or tsA-201 cells were transfected with either $\alpha_2\delta$ cDNA alone or with all calcium channel subunit cDNAs, using the ratios for α1, β, $\alpha_2\delta$, and green fluorescent protein (GFP) of 3:2:2:0.4. For electrophysiological recording, the cDNA for GFP (mut3 GFP) was included in the transfection to identify transfected cells from which recordings were made.

Creation of a tsA-201 stable cell line containing $\alpha_2\delta$-2 with internal HA tag. The internally HA-tagged $\alpha_2\delta$-2 cDNA was cloned in-frame into the mammalian expression vector pcDNA3.1/Zeo(+) (Invitrogen, Carlsbad, CA) using *Kpn*I and *Not*I, linearized with *Pvu*I, and transfected into cultured tsA-201 cells using Fugene 6 (Roche, Mannheim, Germany). The vector conferred Zeocin (Invitrogen) resistance to cells that stably incorporated the plasmid. Clonal foci were isolated using trypsin-impregnated 5-mm-diameter sterile paper discs (Sigma, Poole, UK). Expression of the full-length $\alpha_2\delta$-2 protein was confirmed by Western blotting and functionality of the protein by electrophysiology.

Cholesterol depletion of tsA-201 cells. A 50 mM stock of methyl-β-cyclodextrin (Sigma) was prepared in serum-free medium, sterile filtered, and kept at room temperature for no longer than 10 h. For electrophysiological experiments, cells were replated onto collagen-coated dishes, before addition of methyl-β-cyclodextrin. Cells were treated with methyl-β-cyclodextrin (5 mM) in serum-free medium for 1 h at 37°C (Christian et al., 1997), immediately before use in electrophysiological or biochemical experiments. Control cells were incubated in serum-free medium for the same length of time.

Cell membrane preparation. Membrane fractions from mouse cerebellum or cultured cells were prepared using the following general method. Mouse cerebella were homogenized in a buffer containing the following (in mM): 20 HEPES, pH 7.4, 50 NaCl, 300 sucrose, 2 EDTA, incomplete protease inhibitor cocktail (Roche), and 1 orthophenanthroline. Cultured cell pellets were resuspended in 25 vol of ice-cold 10 mM HEPES, pH 7.4, containing complete protease inhibitor cocktail (Roche). Cells were lysed by 10 passages through a 23 gauge needle, followed by three 10-s rounds of sonication. Cell debris was removed by centrifugation (1000 × *g*, for 15 min at 4°C), and the resultant supernatants were recentrifuged (100,000 × *g*, for 60 min at 4°C) to pellet membranes. Protein concentrations of the membrane preparations were determined by BCA assay (Perbio, Tatenhall, Cheshire, UK). Membranes were used immediately or stored in aliquots at −80°C.

Preparation of Triton X-100-insoluble membrane fraction. All steps were performed on ice. Confluent cells from four 175 cm^2 flasks, or pelleted whole homogenate derived from two mouse cerebella, were taken up in 1.5 ml of MES-buffered saline (MBS) (25 mM MES, pH 6.5, 150 mM NaCl, and complete protease inhibitor cocktail) containing 1% (v/v) Triton X-100 (Perbio), resuspended by five passages through a 23 gauge needle and three 7-s rounds of sonication, and then left on ice for 1 h. An equal volume of 90% (w/v) sucrose in MBS was then added. The 3 ml sample was transferred to a 13 ml ultracentrifuge tube and overlaid with 10 ml of discontinuous sucrose gradient, consisting of 35% (w/v) sucrose in MBS (5 ml) and 5% (w/v) sucrose in MBS (5 ml). The sucrose gradients were centrifuged at 140,000 × *g* for 18 h at 4°C in a Beckman Instruments (Fullerton, CA) SW40 rotor; 1 ml fractions were subsequently harvested from the top to the bottom of the tube. When necessary, protein fractions from the gradient were washed free of sucrose by dilution into 25 vol of MBS and centrifugation (100,000 × *g*, for 60 min at 4°C) to pellet the cholesterol-enriched microdomain material.

Immunoprecipitation. $\alpha_2\delta$-2(HA) was immunoprecipitated from stably transfected tsA-201 cells as follows. Triton X-100-insoluble membranes prepared from these cells were resuspended in immunoprecipitation (IP) solubilization buffer (1% Igepal, 50 mM Tris, 75 mM NaCl, and protease inhibitor cocktail, pH 7.4) for 1 h at 4°C. Insoluble material was removed by centrifugation at 12,000 × *g* at 4°C for 15 min. The clarified material was incubated for 2 h at 4°C with ~2 μg of the appropriate Ab. Protein G-agarose (30 μl of 50% slurry; Sigma) was added and incubated for 1 h at 4°C. Beads were then washed three times in low detergent buffer (0.15% Igepal, 50 mM Tris, 75 mM NaCl, and protease inhibitor cocktail, pH 7.4), and bound protein was removed from the beads by the addition of SDS sample buffer containing 100 mM DTT, with heating at 70°C for 10 min. For protein sequencing, samples were separated on Nu-Page 4–12% Bis-Tris gels (Invitrogen) and stained with Coomassie blue (Simply Blue safe stain; Invitrogen). Bands of interest were excised from the gel, and protein identification was performed at Imperial College London Proteomics Facility by tryptic mass fingerprinting, confirmed by quadrupole time of flight (Q-ToF) mass spectrometry. The probability of correct identification from peptide mass fingerprinting is based on the molecular weight search (MOWSE) score using the Matrix Science Mascot search engine, which is $-10*\mathrm{Log}(P)$, where P is the probability that the observed match is a random event. Individual peptide ion scores >52 indicate identity or extensive homology ($p < 0.05$).

Immunoblotting. Immunoblot analysis was performed essentially as described previously (Page et al., 2004). SDS-PAGE-resolved samples were transferred to polyvinylidene difluoride membranes and probed with relevant primary Abs and the appropriate horseradish peroxidase-conjugated secondary Abs, followed by enhanced chemiluminescence detection. Ca channel and prohibitin primary Abs were used at 1–5 μg/μl, and anti-flotillin-1 and anti-SLP-2 were used at 1:500 and 1:250, respectively.

Electrophysiology. Calcium channel expression in tsA-201 cells was investigated by whole-cell patch-clamp recording. The internal (pipette) and external solutions and recording techniques were similar to those described previously (Campbell et al., 1995). The patch pipette solution contained the following (in mM): 140 Cs-aspartate, 5 EGTA, 2 $MgCl_2$, 0.1 $CaCl_2$, 2 K_2ATP, and 10 HEPES, pH 7.2 (310 mOsm with sucrose). The external solution for recording Ba^{2+} currents contained the following (in mM): 150 tetraethylammonium Br, 3 KCl, 1.0 $NaHCO_3$, 1.0 $MgCl_2$, 10 HEPES, 4 glucose, and 10 $BaCl_2$, pH 7.4 (320 mOsm with sucrose). Pipettes of resistance 2–4 MΩ were used. An Axopatch 1D amplifier (Molecular Devices, Palo Alto, CA) was used, and data were filtered at 1–2 kHz and digitized at 5–10 kHz. Analysis was performed using pClamp7 (Molecular Devices) and Origin 7 (Microcal, Northampton, MA). Current records are shown after leak and residual capacitance current subtraction (P/4 protocol). For determination of the voltage for 50% current activation ($V_{50,act}$), the current density–voltage (*I–V*) relationships were fitted between −30 and +50 mV with a modified Boltzmann equation as follows: $I = G_{max} \times (V - V_{rev})/(1 + \exp(-(V - V_{50,act})/k))$, where I is the current density (in picoamperes per picofarad), G_{max} is the maximum conductance (in nanosiemans per picofarad), V_{rev} is the reversal potential, and k is a slope factor. Steady-state inactivation data

were fitted with a single Boltzmann equation of the following form: $I/I_{max} = ((A_1 - A_2)/[1 + \exp((V - V_{50,inact})/k)] + A_2$, where I_{max} is the maximal current, $V_{50,inact}$ is the half-maximal voltage for current inactivation, and A_1 and A_2 represent the total and non-inactivating current, respectively.

Calcium current recording from isolated Purkinje cells was performed as described previously (Barclay et al., 2001), except for the following points: cerebellar slices (300 μm) were prepared from postnatal days 7–9 mice using a vibrating tissue slicer and kept in 95%O_2/5% CO_2-saturated Krebs' solution for 30 min at 36°C before being cooled to room temperature. Cells were isolated immediately before use by digestion of slices with papain (20 U/ml) for 5–15 min, washed and triturated in Ringer's solution, and plated onto poly-L-lysine-coated coverslips.

Gabapentin binding assay. Binding of [^{3}H]gabapentin was performed as described previously (Canti et al., 2005), in a final volume of 250 μl at room temperature for 2 h. Membranes (50 μg/tube) or cholesterol-rich microdomains (3 μg/tube) were incubated with various concentrations of [^{3}H]gabapentin (ARC, St. Louis, MO) in 10 mM HEPES/KOH, pH 7.4, and then rapidly filtered through GF/B filters, presoaked with 0.3% polyethyleneimine. Filters were washed three times with 3 ml of ice-cold 50 mM Tris/HCl, pH 7.4, and the amount of bound [^{3}H]gabapentin was determined by scintillation counting. Concentrations of [^{3}H]gabapentin >50 nM were achieved by adding nonradioactive gabapentin and correcting the specific binding by the dilution factor, as described previously (Marais et al., 2001). Nonspecific binding was determined in the presence of 1000-fold excess of nonradioactive gabapentin (or pregabalin, with identical results). Replicate (three to five) independent experiments were performed, each in triplicate, and data were analyzed by fitting an equation for a rectangular hyperbola to the specific binding data from each experiment, to obtain the dissociation constant (K_D) and maximum number of binding sites (B_{max}).

Data are presented as mean ± SEM, and statistical significance of differences between data were determined using Student's unpaired, two-tailed *t* test.

Results

Processing of native $\alpha_2\delta$-2 in cerebellar tissue

In parallel with the posttranslational processing that has been determined for native muscle $\alpha_2\delta$-1 (Jay et al., 1991), the theoretical processing of $\alpha_2\delta$-2 is shown in Figure 1*A*. The mature form of $\alpha_2\delta$-2 is thought to be proteolytically cleaved into α_2-2 and δ-2, which remain disulfide bonded, until subjected to disulfide-bond reduction *in vitro* (Hobom et al., 2000; Brodbeck et al., 2002). The cerebellum is rich in native $\alpha_2\delta$-2, and we confirmed that the protein from cerebellum that is recognized by the α_2-2(102–117) Ab used in these studies is indeed derived from $\alpha_2\delta$-2, because it is absent from du^{2J}/du^{2J} cerebellum (Fig. 1*B*). This mouse strain has a 2 bp mutation in the *Cacna2d2* gene (calcium channel, voltage-dependent, alpha2delta subunit-2), which is predicted to result in a complete loss of $\alpha_2\delta$-2 protein (Barclay et al., 2001).

Additional examination of the native species shows it to have the expected molecular mass of ~180 kDa before *in vitro* reduction with DTT and 145 kDa for the reduced form (Fig. 1*A*,*C*). Subsequent *in vitro* deglycosylation with endoglycosidase F (endo-F) resulted in the expected reduction in mass for the reduced α_2-2(102–117)-immunoreactive species from ~145 kDa before deglycosylation to ~107 kDa after deglycosylation (Fig. 1*D*). This is in accordance with the predicted processing shown in the schematic diagram in Figure 1*A*. The specificity of the α_2-2(102–117) Ab was further confirmed by showing that it recognized heterologously expressed $\alpha_2\delta$-2 but not $\alpha_2\delta$-1 or $\alpha_2\delta$-3 transfected into tsA-201 cells (data not shown).

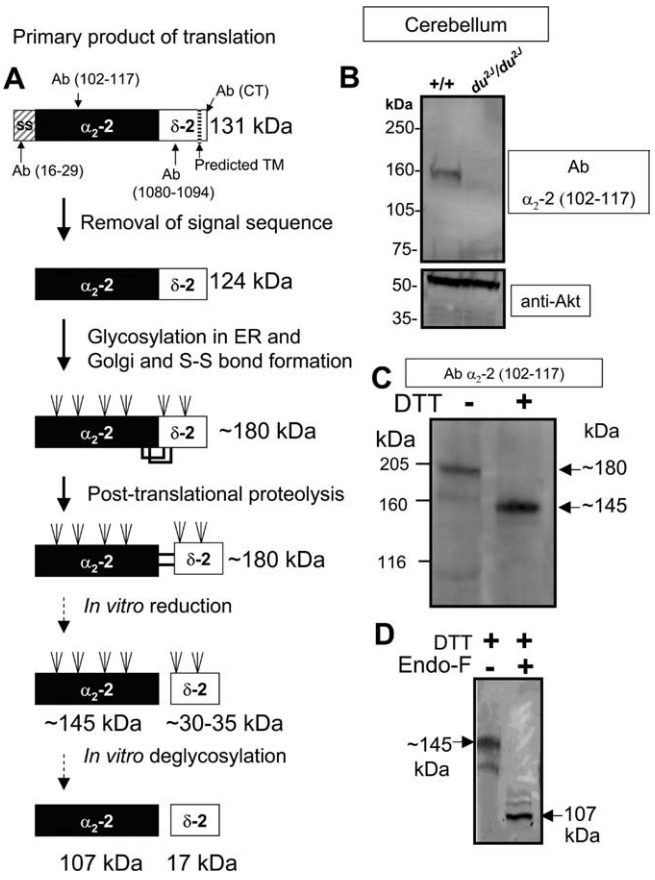

Figure 1. Processing of $\alpha_2\delta$-2 from cerebellum. ***A***, Schematic showing the proposed products of posttranslational and *in vitro* modifications of the $\alpha_2\delta$-2 subunit. SS, Signal sequence; S-S, disulfide bond; TM, transmembrane domain. ***B***, Presence of α_2-2(102–117)-immunoreactive band in wild-type but absence from du^{2J}/du^{2J} cerebellar membranes, separated under reducing conditions, in the presence of DTT (100 mM). Akt immunoreactivity was used as a loading control. ***C***, Western blot of cerebellar membranes separated under nonreducing conditions (−) or reducing conditions (+100 mM DTT) and probed with Ab α_2-2(102–117). Immunolabeled bands corresponding to mature full-length $\alpha_2\delta$-2 (~180 kDa) and glycosylated α_2-2 (~145 kDa) are arrowed. ***D***, Western blot of cerebellar membranes prepared under reducing conditions, treated without (−) or with (+) endo-F and then probed with Ab α_2-2(102–117). Bands corresponding to glycosylated α_2-2 and deglycosylated α_2-2 (107 kDa) are arrowed.

Native $\alpha_2\delta$-2 from cerebellum is colocalized in cholesterol-rich microdomains with $Ca_V2.1$

The punctate cell-surface distribution of heterologously expressed $\alpha_2\delta$-2 that we observed previously after heterologous expression of $\alpha_2\delta$-2 (Canti et al., 2005) suggested to us that it might be concentrated in cholesterol-rich microdomains. Cell lysates were prepared from mouse cerebellum and separated on a sucrose gradient. These showed native $\alpha_2\delta$-2 to be entirely concentrated in cholesterol-rich lipid raft microdomains (Fig. 2*A*, fractions 5, 6), in which it colocalizes with the lipid raft marker flotillin-1 (Fig. 2*A*). Within the lipid raft fraction, $\alpha_2\delta$-2 is entirely in its mature disulfide-bond linked form, as shown by the fact that, when subjected to SDS-PAGE under reducing conditions, it is separated into α_2-2 (~145 kDa) (Fig. 2*A*,*B*) and δ-2 (~32 kDa) (Fig. 2*B*) and, as expected, has a cleaved signal sequence (Fig. 2*B*). No $\alpha_2\delta$-2 was present in the Triton X-100-soluble fraction (Fig. 2*A*, fractions 10–13). We also examined the distribution of native $Ca_V2.1$ in the cerebellar sucrose gradient fractions and found that it substantially colocalized with $\alpha_2\delta$-2 in the cholesterol-rich microdomain fractions, although some was

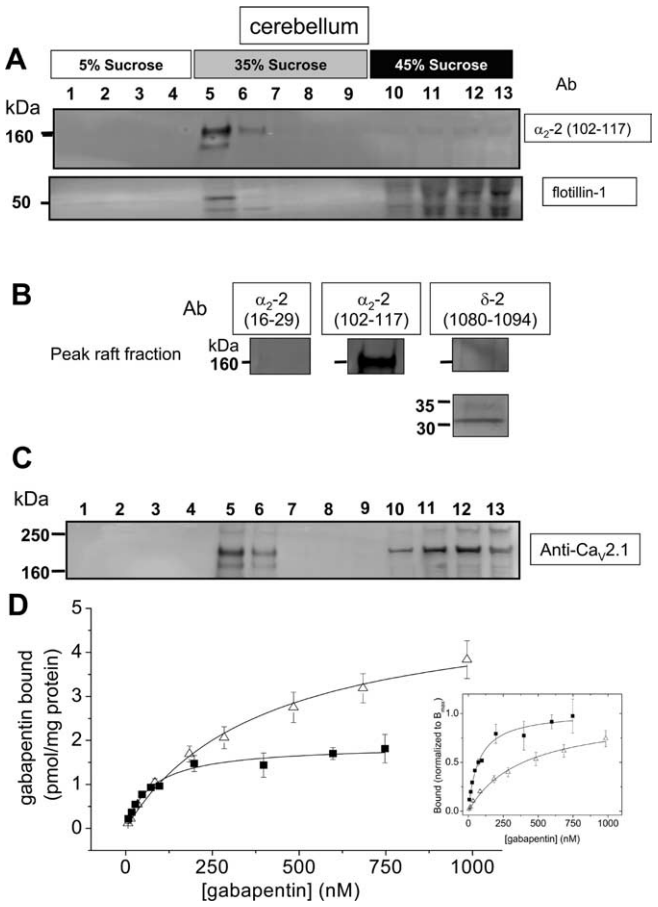

Figure 2. Presence of $\alpha_2\delta$-2 and $Ca_V2.1$ in cholesterol-rich microdomains from mouse cerebellum. ***A***, Western blot analysis of the distribution of proteins from a typical discontinuous sucrose gradient derived from whole cerebellar homogenate. Fractions under reducing conditions were probed with Ab α_2-2(102–117) (top) and anti-flotillin-1 (bottom). ***B***, The flotillin-1-positive peak fraction from the sucrose gradient shown in ***A*** was further characterized using Abs α_2-2(16–29) (left), α_2-2(102–117) (middle), and δ-2(1080–1094) (right). ***C***, Western blot analysis of the distribution of $Ca_V2.1$ from the same sucrose gradient as in ***A***. Fractions under reducing conditions were probed with anti $Ca_V2.1$ Ab. ***D***, Measurement of the affinity of [^{3}H]gabapentin binding sites in a membrane fraction (△; fitted to a hyperbola with K_D 392 nM, mean of $n = 3$) and cholesterol-rich microdomains (■; fitted to a hyperbola with K_D 74.6 nM, mean of $n = 3$) derived from mouse cerebellum. Data in the inset graph have been normalized to each mean B_{max} to illustrate the difference in K_D values.

also present in the Triton X-100-soluble fractions (fractions 10–13), which contain a large percentage of the total protein (Fig. 2*C*) (for quantification, see Fig. 6*A*). Two main immunoreactive bands were observed for $Ca_V2.1$, of mass ~250 and 190 kDa, with the lower band being the predominant species. Multiple mass species of $Ca_V2.1$ have been attributed previously to the existence of different C-terminal splice variants and to proteolytic cleavage of the C terminus (Sakurai et al., 1995). Furthermore, there is evidence that these species may have differing locations (Sakurai et al., 1996).

Gabapentin binding to cerebellar $\alpha_2\delta$-2 is enhanced in cholesterol-rich microdomains

Gabapentin is a ligand for $\alpha_2\delta$-2 as well as $\alpha_2\delta$-1 (Canti et al., 2003, 2005; Klugbauer et al., 2003). We therefore examined the [^{3}H]gabapentin binding affinity in cholesterol-rich microdomains compared with membrane preparations from cerebellum. The affinity for [^{3}H]gabapentin was increased 4.8-fold in the lipid raft fraction, with the K_D being reduced from 385 ± 56 nM in membranes ($n = 3$) to 79.7 ± 19.8 nM ($n = 3$) in lipid rafts (Fig. 2*D*). The B_{max} was 5.23 ± 0.73 pmol/mg protein in cerebellar membranes and 1.67 ± 0.45 pmol/mg protein for cerebellar rafts.

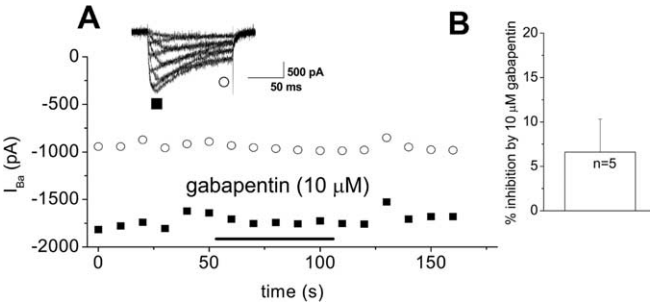

Figure 3. Lack of effect of gabapentin on calcium channel currents recorded from cerebellar Purkinje cells. ***A***, Example of the lack of effect of gabapentin (10 μM) on the time course of calcium channel currents recorded from a holding potential of −90 mV to a test potential of +20 mV, every 10 s from an isolated cerebellar Purkinje cell, measured at peak (■) and end (○) of pulse. The inset shows current traces from a current–voltage relationship performed before the time course, with voltage pulses of −50 to +30 mV in 10 mV steps. Gabapentin application is indicated by the horizontal bar. ***B***, Inhibition (mean ± SEM) by gabapentin (10 μM) (white bar).

Gabapentin has no acute effect on Purkinje cell calcium currents

It is assumed in much of the literature that gabapentin has its effect via binding to $\alpha_2\delta$ subunits and consequently inhibiting calcium currents (for review, see Sutton and Snutch, 2001) and reducing transmitter release (van Hooft et al., 2002). However, the effect of gabapentin on calcium currents is controversial because, although it has been found to produce a small inhibition of native calcium currents in sensory neurons (Sutton et al., 2002), it does not produce acute inhibition of calcium currents in heterologous expression systems (Vega-Hernandez and Felix, 2002; Canti et al., 2003). Because $\alpha_2\delta$-2 is very strongly expressed in cerebellar Purkinje cells (Barclay et al., 2001) and has also been found to be associated with many other GABAergic neurons (Cole et al., 2005), we therefore examined the effect of gabapentin on Purkinje cell calcium currents. An inhibition of calcium currents in GABAergic neurons and consequent inhibition of GABA release would not be compatible with the well established antiepileptic action of gabapentin. We found no significant effect of 1–10 μM gabapentin on Purkinje cell calcium currents from wild-type mice (Fig. 3*A*,*B*).

Colocalization of heterologously expressed $Ca_V\alpha1$ subunits with $\alpha_2\delta$-2 in cholesterol-rich microdomains

We wanted to examine whether heterologously expressed $\alpha_2\delta$-2 was also localized in lipid rafts in a similar manner to native $\alpha_2\delta$-2. For these experiments, we used either transient transfection of wild-type $\alpha_2\delta$-2 or a cell line stably expressing either wild-type $\alpha_2\delta$-2 or $\alpha_2\delta$-2 with an internal HA tag [$\alpha_2\delta$-2(HA)].

It was first important to determine whether $\alpha_2\delta$-2 with an internal HA tag was fully functional. Coexpression of $\alpha_2\delta$-2 enhanced calcium currents through all HVA calcium channels in all expression systems we tested (Canti et al., 2005). In the example shown in Figure 4, *A* and *B*, $\alpha_2\delta$-2 increased currents through $Ca_V2.1/\beta4$ channels in tsA-201 cells by 3.8 fold ($n = 16$). This is a physiologically relevant subunit combination, likely to be the main functional heteromeric calcium channel in cerebellar Purkinje cells. Transient transfection of the $\alpha_2\delta$-2(HA) construct enhanced $Ca_V2.1/\beta4$ currents to the same extent as wild-type

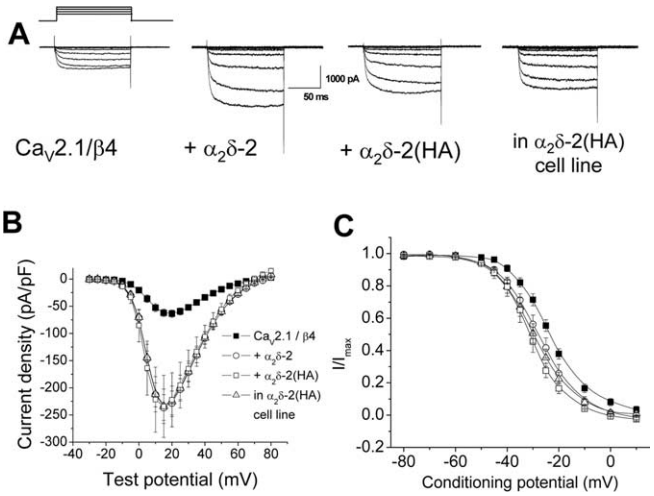

Figure 4. Comparison of the effect of expression of $\alpha_2\delta$-2 and $\alpha_2\delta$-2(HA) on currents through $Ca_v2.1/\beta4$ channels in tsA-201 cells. $Ca_v2.1/\beta4$ were expressed alone or with $\alpha_2\delta$-2 or $\alpha_2\delta$-2 with internal HA tag [$\alpha_2\delta$-2(HA)] in tsA-201 cells, and currents were recorded using Ba^{2+} as charge carrier. ***A***, Representative current traces elicited between −30 and +15 mV in 5 mV steps from a holding potential of −90 mV for $Ca_v2.1/\beta4$ (left), $Ca_v2.1/\beta4/\alpha_2\delta$-2 (middle left), $Ca_v2.1/\beta4/\alpha_2\delta$-2(HA) (middle right), or $Ca_v2.1/\beta4$ in stable $\alpha_2\delta$-2(HA) cell line (right). ***B***, Current density–voltage relationships (mean ± SEM) for the four experimental conditions. ■, $Ca_v2.1/\beta4$ ($n = 13$); ○, with $\alpha_2\delta$-2 ($n = 16$); □, with $\alpha_2\delta$-2(HA) ($n = 7$); △, $Ca_v2.1/\beta4$ in $\alpha_2\delta$-2(HA) cell line ($n = 21$). ***C***, Steady-state inactivation (mean ± SEM) for the four experimental conditions: $Ca_v2.1/\beta4$ (■; $n = 7$; $V_{50} = -23.7 \pm 1.2$ mV); with $\alpha_2\delta$-2 (○; $n = 2$; $V_{50} = -27.3$ mV); with $\alpha_2\delta$-2(HA) (□; $n = 3$; $V_{50} = -30.6 \pm 1.9$ mV; $p < 0.01$ compared with no $\alpha_2\delta$-2), and $Ca_v2.1/\beta4$ in $\alpha_2\delta$-2(HA) cell line (△; $n = 8$; $V_{50} = -29.5 \pm 1.9$ mV; $p < 0.03$ compared with no $\alpha_2\delta$-2).

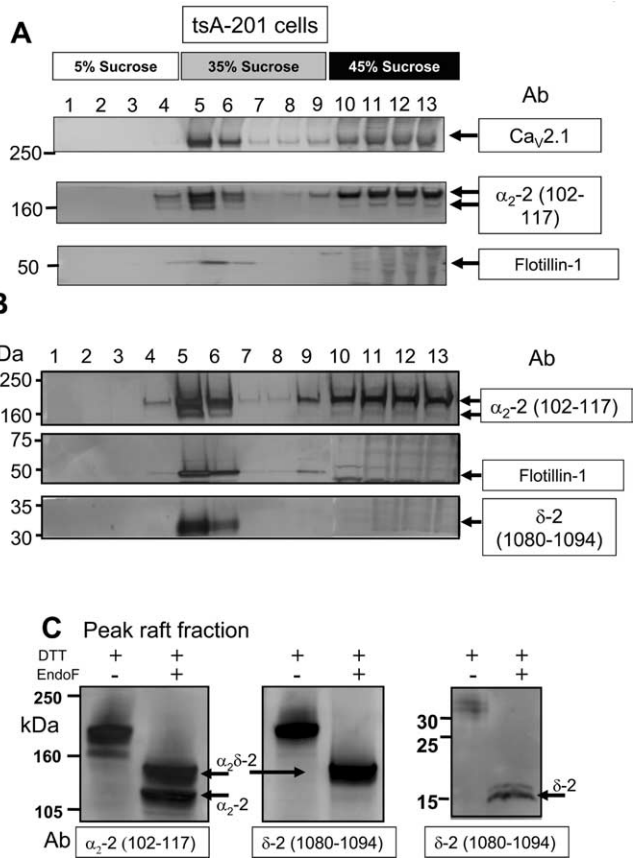

Figure 5. Colocalization of $\alpha_2\delta$-2 and $Ca_V2.1$ in cholesterol-rich microdomains from $\alpha_2\delta$-2(HA) cell line. ***A***, Stably transfected tsA-201 cells containing $\alpha_2\delta$-2(HA) were transiently transfected with $Ca_v2.1$ and $\beta4$, and Western blot analysis was performed of the distribution of proteins found in fractions from a typical discontinuous sucrose gradient. Fractions (separated on SDS-PAGE under disulfide-bond-reducing conditions) were probed for $Ca_V2.1$ (top) and $\alpha_2\delta$-2 with Ab α_2-2(102–117) (middle). The bottom shows the location of the cholesterol-rich microdomain marker protein flotillin-1 (arrowed). ***B***, Western blot analysis was performed as in ***A***, except that the $\alpha_2\delta$-2(HA) cell line was not additionally transfected with other subunits. Fractions (separated under disulfide-bond-reducing conditions) were probed for $\alpha_2\delta$-2-derived products with Abs α_2-2(102–117) and δ-2(1080–1094) (top and bottom). The middle shows the location of the cholesterol-rich microdomain marker protein flotillin-1 (arrowed). For Ab α_2-2(102–117), the top and bottom arrows indicate bands corresponding in size to the nonreducible full-length $\alpha_2\delta$-2 (~180 kDa) and free α_2-2 (145 kDa) proteins, respectively. For Ab δ-2(1080–1094), the arrow indicates free δ-2 peptide (32 kDa). ***C***, Aliquots of the peak lipid raft fraction from the sucrose gradient in ***B*** were treated *in vitro* under reducing conditions without (−) or with (+) endo-F, and the products were analyzed on Western blots with Abs α_2-2(102–117) (left) and δ-2(1080–1094) (middle and right). The positions of bands corresponding in size to nonreducible deglycosylated full-length $\alpha_2\delta$-2 and deglycosylated free α_2-2 are indicated with arrows (left and middle). A band corresponding to deglycosylated δ-2 peptide is arrowed in the right.

$\alpha_2\delta$-2, and these currents were very similar to those obtained after transient transfection of $Ca_V2.1/\beta4$ into the stable $\alpha_2\delta$-2(HA) cell line (Fig. 4*B*). Furthermore, both $\alpha_2\delta$-2 and $\alpha_2\delta$-2(HA) produced a similar small hyperpolarization of the steady-state inactivation compared with $Ca_V2.1/\beta4$ alone (Fig. 4*C*).

The processing of stably expressed $\alpha_2\delta$-2(HA) was examined in either the additional presence of transiently transfected $Ca_V2.1$ and $\beta4$ (Fig. 5*A*) or their absence (Fig. 5*B*). Cells were lysed, and the Triton X-100-soluble and -insoluble fractions were separated on a discontinuous sucrose gradient. Fractions from the sucrose gradient were analyzed by SDS-PAGE under reducing conditions in the presence of DTT. As was the case for cerebellar $\alpha_2\delta$-2, the heterologously expressed $\alpha_2\delta$-2 was clearly present in the flotillin-1-positive lipid raft fractions (Fig. 5*A*,*B*, fractions 5, 6), although it was also present in the Triton X-100 soluble fractions (fractions 10–13). This was true in both the presence (Fig. 5*A*) and absence (Fig. 5*B*) of coexpressed $Ca_V2.1$.

Whereas a single α_2-2(102–117)-immunoreactive band of ~180 kDa was predominant in the Triton X-100-soluble fractions (fractions 10–13), two bands of ~180 and 145 kDa were present in the lipid raft fractions 5 and 6 (Fig. 5*A*,*B*), which are likely to represent intact noncleaved $\alpha_2\delta$-2 and fully mature α_2-2 derived from disulfide-bonded $\alpha_2\delta$-2, respectively. In agreement with this, a δ-2(1080–1094)-immunoreactive band at ~32 kDa was only observed in the lipid raft fractions (Fig. 5*B*). Similar results were obtained using transient transfection of wild-type $\alpha_2\delta$-2, indicating that this partial processing of heterologously expressed $\alpha_2\delta$-2 is not a result of introduction of the HA tag (data not shown).

Additional investigation of the peak lipid raft fraction was undertaken to confirm the nature of the two protein bands that were immunoreactive against α_2-2(102–117), by subjecting this fraction to *in vitro* deglycosylation before separation under reducing conditions on SDS-PAGE (Fig. 5*C*). Deglycosylation tended to increase the immunoreactivity with the anti-peptide Abs, probably by increasing the exposure of the peptide epitopes. This analysis showed that the 180 and 145 kDa bands were reduced in mass to ~125 and 107 kDa after *in vitro* deglycosylation (Fig. 5*C*, left panel), consistent with their identification as full-length $\alpha_2\delta$-2 and free α_2-2. Additional confirmation of this conclusion is that only the upper band is immunoreactive against the δ-2(1080–1094) Ab (Fig. 5*C*, middle panel). Free δ-2 is also present (Fig. 5*C*, right panel).

We also observed that a substantial proportion of coexpressed $Ca_V2.1$ was present in the Triton X-100-insoluble lipid raft frac-

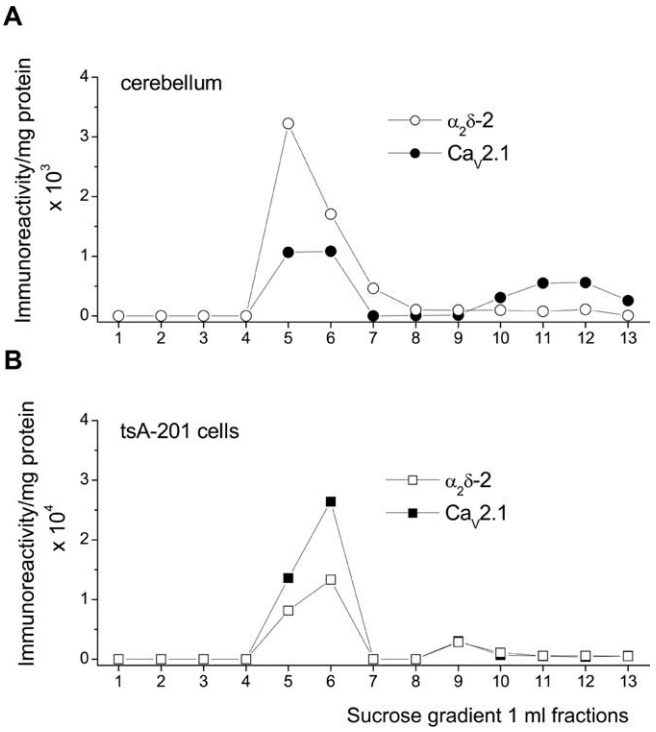

Figure 6. Quantification of the localization of $\alpha_2\delta$-2 and $Ca_V2.1$ in cholesterol-rich microdomains. The presence of $\alpha_2\delta$-2 (open symbols) and $Ca_V2.1$ (filled symbols) in sucrose gradient fractions from cerebellum (***A***, circles) and tsA-201 cells (***B***, squares). The band intensities were quantified using ImageQuant5.2 (Molecular Dynamics, Sunnyvale, CA) and expressed as arbitrary density units per milligram of protein in each fraction.

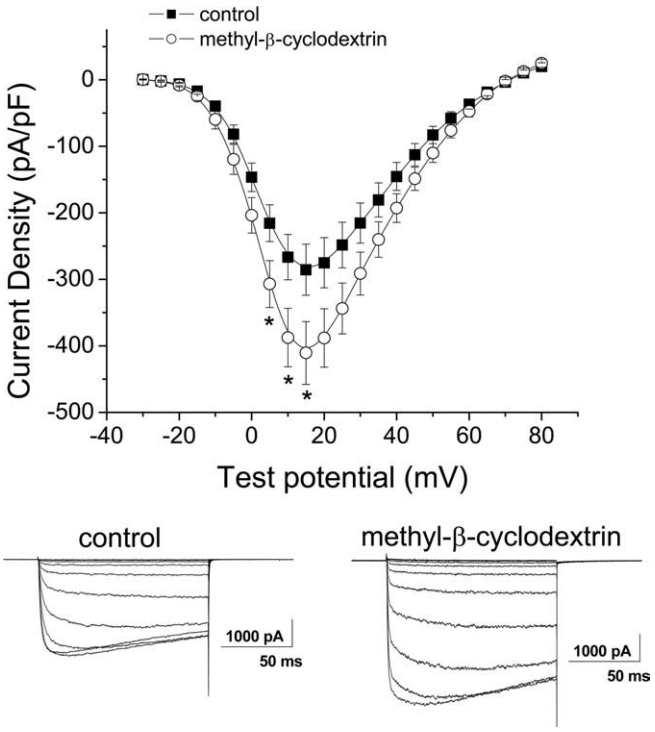

Figure 7. Effect of cholesterol depletion with methyl-β-cyclodextrin on calcium channel currents. $Ca_V2.1/\beta4$ were expressed in the stable $\alpha_2\delta$-2(HA) cell line and current density–voltage relationships (mean ± SEM; top) were determined in parallel, either after treatment with methyl-β-cyclodextrin (5 mM) for 1 h at 37°C (○; $n = 17$) or after identical treatment without methyl-β-cyclodextrin (■; $n = 17$). *$p < 0.05$, Student's unpaired t test. Bottom, Example traces under the two conditions, from a holding potential of −90 mV to test potentials of between −30 and +15 mV at 5 mV intervals.

tions in tsA-201 cells (Fig. 5*A*). In this study, the long C-terminal isoform of $Ca_V2.1$ was expressed, and the mass of ~250 kDa is in agreement with its predicted mass. To compare the localization in lipid rafts of $Ca_V2.1$ and $\alpha_2\delta$-2 in cerebellum and tsA-201 cells, we quantified the α_2-2(102–117) and $Ca_V2.1$ immunoreactivity in the sucrose gradient fractions per milligram of total protein (Fig. 6). This shows that $\alpha_2\delta$-2 is strongly concentrated in the lipid raft fraction in both cerebellum (Fig. 6*A*) and tsA-201 cells (Fig. 6*B*), whereas $Ca_V2.1$ is more strongly concentrated in lipid raft fractions in tsA-201 cells than in cerebellum. This suggests that, in cerebellum, some $Ca_V2.1$ is either associated with an $\alpha_2\delta$ that is not concentrated in lipid rafts or that not all native $Ca_V2.1$ is associated with $\alpha_2\delta$. In this regard, we observed that $\alpha_2\delta$-1 is also associated with lipid rafts (data not shown). It is therefore possible that some native $Ca_V2.1$ is not associated with these $\alpha_2\delta$ subunits.

Effect of cholesterol depletion of tsA-201 cells

The $\alpha_2\delta$-2(HA) tsA-201 cell line was incubated with methyl-β-cyclodextrin (5 mM) for 1 h to deplete membrane cholesterol (Christian et al., 1997), and calcium channel currents were recorded in cells that had also been transiently transfected with $Ca_V2.1$ and $\beta4$ (Fig. 7). Lipid rafts became disrupted by the methyl-β-cyclodextrin treatment, as shown previously (Fagan et al., 2000). We confirmed there was a reduced concentration of flotillin-1 in the Triton X-100-insoluble fraction (data not shown). Calcium channel currents were significantly elevated after cholesterol depletion (Fig. 7). The increase at +15 mV was 44.1 ± 16.5% ($n = 17$; $p < 0.05$). There was no effect on the $V_{50,act}$, which was +2.8 ± 1.2 mV after treatment with cyclodextrin compared with +3.7 ± 0.8 mV for controls performed in parallel ($n = 17$ for both).

Coimmunoprecipitation of $\alpha_2\delta$-2 with other lipid raft constituent proteins

We examined whether $\alpha_2\delta$-2 is associated with other protein constituents of lipid rafts and found that IP of $\alpha_2\delta$-2(HA) from the lipid raft fraction, by means of its HA tag, consistently resulted in coimmunoprecipitation with three related proteins of the SPFH family (stomatin/prohibitin/flotillin/HflK), which have been identified to be lipid raft constituent proteins (for review, see Langhorst et al., 2005). They were identified by peptide mass fingerprinting and Q-ToF mass spectrometry. The proteins identified were SLP-2 (Owczarek et al., 2001), which was present in the excised ~60 kDa band, presumably complexed to another protein or as a dimer, because its monomer protein mass is 39 kDa. Three peptides were identified for this protein giving an MOWSE score of 85 ($p < 0.05$). Stomatin (for review, see Rivera-Milla et al., 2006) was identified to be present in the excised ~40 kDa band. Four peptides were identified for stomatin, giving an MOWSE score of 108 ($p < 0.05$). Prohibitin was also identified in the excised 40 kDa band, with an MOWSE score of 285 ($p < 0.05$), and, in addition, the same protein was identified in the excised ~32 kDa band, which is similar to its protein mass of 30 kDa (Fig. 8*A*). We found that SLP-2 is strongly, although not exclusively, expressed in the peak Triton X-100-insoluble lipid rafts from tsA-201 cells (Fig. 8*B*), as is prohibitin (data not shown). Immunoprecipitation of $\alpha_2\delta$-2, followed by immunoblotting confirmed the presence of coimmunoprecipitating

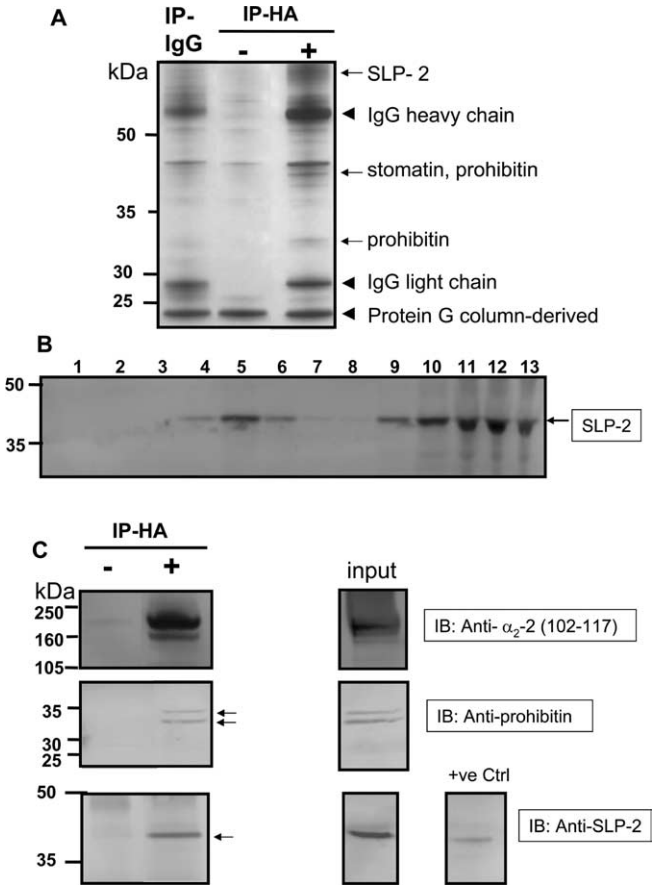

Figure 8. Coimmunoprecipitation of $\alpha_2\delta$-2(HA) with stomatin, SLP-2, and prohibitin. ***A***, Silver stain showing proteins coimmunoprecipitating with $\alpha2\delta$-2(HA) from the $\alpha_2\delta$-2(HA) cell line using an anti-HA Ab (right lane) and the α_2-2(102–117) Ab (data not shown) for immunoprecipitation. Bands indicated with arrows that were absent from the lanes showing proteins immunoprecipitated with control IgG (left lane) or no Ab (middle lane) were excised and identified as described in Materials and Methods. The nonspecific IgG heavy (55 kDa) and light (28 kDa) chains and a protein G-column-derived band (15 kDa) are also indicated with arrowheads. ***B***, Western blot analysis was performed of the distribution of SLP-2 (arrowed) in fractions from a typical discontinuous sucrose gradient. ***C***, Anti-HA Ab was used to immunoprecipitate $\alpha_2\delta$-2(HA) from lipid rafts (top). The input is shown on the right. Prohibitin was coimmunoprecipitated from lipid rafts with the anti-HA Ab (middle lane; two bands arrowed) and was absent from the control IP (left lane). SLP-2 was also coimmunoprecipitated from lipid rafts with $\alpha_2\delta$-2(HA), using either the δ-2 (CT) Ab (data not shown) or the anti-HA Ab (bottom). SLP-2 was absent from the control IP (left) and present in the input and in the positive control supplied with the SLP-2 Ab (human epidermoid carcinoma cell line lysate).

SLP-2 and prohibitin (Fig. 8*C*). No commercial Ab was available for stomatin, and thus its interaction with $\alpha_2\delta$-2 has not yet been verified by immunoblotting.

Gabapentin binding to heterologously expressed $\alpha_2\delta$-2 is enhanced in cholesterol-rich microdomains

For comparison with cerebellum, we examined the concentration of [^{3}H]gabapentin binding sites and their affinity for [^{3}H]gabapentin in cholesterol-rich microdomains compared with membrane preparations, both derived from the $\alpha_2\delta$-2(HA) cell line (Fig. 9*A*).

Initial studies showed that the presence of the HA tag had no effect on the gabapentin binding affinity. For wild-type $\alpha_2\delta$-2, stably expressed in tsA-201 cells, the apparent K_D for [^{3}H]gabapentin in membranes was 450.6 ± 36.9 nM ($n = 4$), very similar to the apparent K_D for gabapentin binding to membranes prepared from the $\alpha_2\delta$-2(HA) cell line, which was 474.4 ± 32.9 nM ($n = 3$).

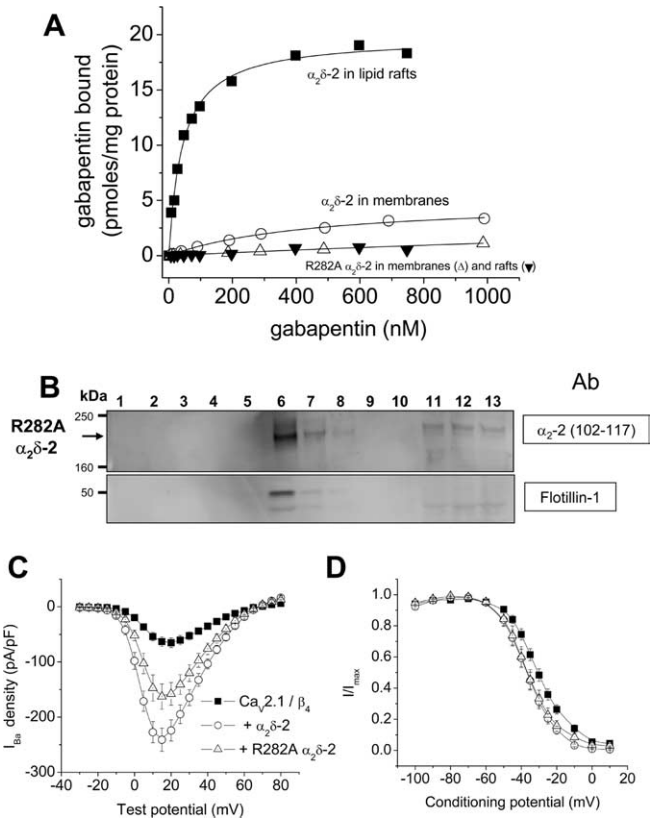

Figure 9. Gabapentin binding to $\alpha_2\delta$-2(HA) cell line is enhanced in cholesterol-enriched microdomains and prevented by R282A mutation. ***A***, Examples of experiments to determine the concentration of [^{3}H]gabapentin binding sites and affinity for [^{3}H]gabapentin of a membrane fraction (○; K_D of 468 nM; representative example from $n = 3$) and cholesterol-rich microdomains (■; K_D of 42.6 nM; representative example from $n = 4$) derived from the $\alpha_2\delta$-2(HA) cell line. Also included on this graph are examples of the lack of binding of [^{3}H]gabapentin to membranes (△; representative example from $n = 5$) or lipid rafts (▼; representative example from $n = 2$) prepared from Cos-7 cells transiently expressing the R282A $\alpha_2\delta$-2 mutant. ***B***, Western blot analysis of the distribution of proteins found in fractions from a typical discontinuous sucrose gradient, derived from transient expression of R282A $\alpha_2\delta$-2. Fractions 1–13 from the sucrose gradient (run under disulfide-bond-reducing conditions) were probed for $\alpha_2\delta$-2-derived products with Ab α_2-2(102–117) (top). The bottom shows the location of the cholesterol-rich microdomain marker protein flotillin-1. ***C***, Comparison of the effect of expression of $\alpha_2\delta$-2 and R282A $\alpha_2\delta$-2 on currents through $Ca_V2.1/\beta4$ channels in tsA-201 cells, using Ba^{2+} as charge carrier. Current density–voltage relationships (mean ± SEM) are shown for the three experimental conditions: ■, $Ca_V2.1/\beta4$ ($n = 14$); ○, with $\alpha_2\delta$-2 ($n = 14$); and △, with R282A $\alpha_2\delta$-2 ($n = 18$). ***D***, Comparison of the effect of expression of $\alpha_2\delta$-2 and R282A $\alpha_2\delta$-2 on the steady-state inactivation of currents through $Ca_V2.1/\beta4$ channels in tsA-201 cells. Conditioning prepulses of 5 s to the potentials shown were given before a constant test pulse to +10 mV. The normalized data (mean ± SEM) are shown for the three experimental conditions: ■, $Ca_V2.1/\beta4$ ($n = 11$); ○, with $\alpha_2\delta$-2 ($n = 11$); and △, with R282A $\alpha_2\delta$-2 ($n = 9$). The V_{50} values are −30.5 ± 0.4, −36.2 ± 0.5, and −36.5 ± 0.4 mV, and the k values are 8.4 ± 0.4, 8.0 ± 0.4, and 8.1 ± 0.4 mV, respectively.

Just as we observed in the cerebellum, the affinity for [^{3}H]gabapentin was enhanced in the lipid raft fraction compared with the membrane fraction. The affinity of $\alpha_2\delta$-2(HA) for [^{3}H]gabapentin was approximately ninefold greater in the cholesterol-rich microdomain fraction compared with the membrane fraction, the apparent K_D decreasing to 53.3 ± 8.4 nM ($n = 4$). Unlike in the cerebellum, the B_{max} also increased from 5.1 ± 0.4 pmol/mg protein ($n = 3$) in the membrane fraction to 71.1 ± 29.8 pmol/mg protein ($n = 4$) in the lipid raft fraction, indicating a 14-fold purification of [^{3}H]gabapentin binding sites in this fraction. No specific [^{3}H]gabapentin binding was observed in the absence of transfected $\alpha_2\delta$-2 (data not shown). One explanation

for the increase in B_{max} is that it may relate to the lower relative concentration of total protein in the lipid raft fraction of the tsA-201 cell line.

The effect of a mutation R282A in $\alpha_2\delta$-2 that prevents [^{3}H]gabapentin binding

The binding of [^{3}H]gabapentin was almost completely abrogated by a mutation R282A in $\alpha_2\delta$-2, which is situated just before the VWA domain. The affinity for [^{3}H]gabapentin was reduced very substantially by this mutation to an unmeasurably high K_D of >2 μM ($n = 5$) (Fig. 9*A*). Although the R282A mutant $\alpha_2\delta$-2 did partition into cholesterol-rich microdomains (Fig. 9*B*), its affinity for gabapentin was not enhanced in this fraction (Fig. 9*A*). An equivalent R217A mutation in $\alpha_2\delta$-1 has been described previously to prevent [^{3}H]gabapentin binding to $\alpha_2\delta$-1 (Wang et al., 1999), and a knock-in mouse carrying this mutation has been reported to be nonresponsive to gabapentin (Taylor, 2004). We confirmed that the R282A mutant $\alpha_2\delta$-2 was still functional, although it enhanced $Ca_V2.1/\beta4$ currents to a significantly smaller extent than wild-type $\alpha_2\delta$-2 in tsA-201 cells. The peak I_{Ba} at +15 mV was enhanced only 2.6-fold by R282A $\alpha_2\delta$-2 compared with 3.8-fold for wild-type $\alpha_2\delta$-2 ($p < 0.05$) (Fig. 9*C*). However, both the wild-type and R282A $\alpha_2\delta$-2 hyperpolarized the steady-state inactivation to similar extents, indicating that, despite a reduction in the peak currents, the R282A mutant $\alpha_2\delta$-2 is still able to influence the properties of the expressed channels (Fig. 9*D*). For $\alpha_2\delta$-1, hyperpolarization of the steady-state inactivation was found to be a property of the δ subunit (Felix et al., 1997).

Discussion

Previous *in vitro* studies have shown that $\alpha_2\delta$-1, $\alpha_2\delta$-2, and $\alpha_2\delta$-3 subunits all increase the maximum conductance of a number of expressed calcium channel $\alpha1/\beta$ subunit combinations at the whole-cell level in several different expression systems (Mori et al., 1991; Gurnett et al., 1996; Walker and De Waard, 1998; Klugbauer et al., 1999; Hobom et al., 2000; Barclay et al., 2001). However, this may be dependent to some extent on the specific combination of $\alpha1$ and β subunits expressed (Klugbauer et al., 1999). Furthermore, the effects of $\alpha_2\delta$ subunits on the kinetics and voltage dependence of inactivation, while present, are relatively minor (Walker and De Waard, 1998; Klugbauer et al., 1999; Canti et al., 2003). We previously investigated the effect of $\alpha_2\delta$-2 on currents resulting from several combinations of Ca_V $\alpha1$ and β subunits and have shown that, whereas there was an approximately threefold increase in maximum whole-cell conductance (Barclay et al., 2001; Canti et al., 2005), $\alpha_2\delta$-2 had no influence on single-channel conductance (Barclay et al., 2001; Brodbeck et al., 2002). This implies that $\alpha_2\delta$-2 probably has its main effect on the number of channel complexes in the plasma membrane, either by enhancing trafficking to the plasma membrane or reducing turnover of channels. In agreement with this proposed mechanism, it has been found previously that $\alpha_2\delta$-1 increased the amount of $Ca_V1.2$ protein expressed in *Xenopus* oocytes (Shistik et al., 1995). We have shown recently that the MIDAS motif in the VWA domain within $\alpha_2\delta$-2 is of key importance in trafficking $Ca_V\alpha1$ subunits (Canti et al., 2005).

Localization of $\alpha_2\delta$-2 in lipid microdomains

In the present study, we have shown that $\alpha_2\delta$-2 from cerebellum partitions completely into the Triton X-100-insoluble lipid raft fraction. Flotillin-1 was used as a marker of the lipid raft fraction, because it shows ubiquitous tissue expression (for review, see Morrow and Parton, 2005; Rivera-Milla et al., 2006), whereas caveolins, which are markers for the caveolar lipid rafts, have been reported to be absent or poorly expressed in brain (Scherer et al., 1996).

We also found $\alpha_2\delta$-2 to be strongly concentrated in the lipid raft fractions isolated from an $\alpha_2\delta$-2(HA)-expressing cell line, in which the mature species that is proteolytically processed into α_2-2 and δ-2 is only present in these cholesterol-rich microdomains. In addition, $Ca_V2.1$ was concentrated with $\alpha_2\delta$-2 in lipid rafts when expressed in tsA-201 cells and to a lesser extent in cerebellum. Evidence that association with cholesterol-rich microdomains is of functional importance comes from our finding that depletion of cholesterol from intact cells significantly enhanced $Ca_V2.1/\alpha_2\delta$-2/$\beta4$ calcium channel currents. In general agreement with this, it has been shown that native N-type channel activity is reduced by enhancing membrane cholesterol (Toselli et al., 2005). Of relevance to the localization of calcium channel complexes in specific membrane microdomains, $Ca_V2.1$ has also been found to localize in synaptosomal lipid rafts with certain SNARE (soluble *N*-ethylmaleimide-sensitive factor attached protein receptor) complex proteins (Taverna et al., 2004), whereas a similar localization was not identified for L-type channels.

Additional evidence that $\alpha_2\delta$-2 interacts with other lipid raft constituent proteins comes from the proteomic identification of several proteins of the SPFH family: SLP-2, stomatin, and prohibitin, which coimmunoprecipitate with $\alpha_2\delta$-2. These proteins are submembrane scaffold proteins that are known constituents of lipid rafts in both the plasma membrane and endocytic vesicles (Foster et al., 2003; Langhorst et al., 2005; Morrow and Parton, 2005; Rivera-Milla et al., 2006). Furthermore, a stomatin homolog in *Caenorhabditis elegans* [MEC-2 (mechanotransducing channel subunit-2)] was identified to be involved in mechanosensation (Chalfie and Au, 1989). However, whereas MEC-2 enhanced *C. elegans* degenerin/epithelial Na^+ channel (DEG/ENac) currents (Goodman et al., 2002), stomatin inhibited the related mammalian ASIC3 acid-sensing ion channels (Price et al., 2004). The functional importance of the interaction between $\alpha_2\delta$-2 and proteins of the SPFH family, and whether it is direct, remains to be determined. However, it is of interest that a role for the related lipid raft protein flotillin in endocytosis has recently been defined (Glebov et al., 2006).

Affinity of gabapentin binding to $\alpha_2\delta$-2 is enhanced in lipid rafts

Gabapentin is a ligand for $\alpha_2\delta$-2 as well as $\alpha_2\delta$-1, and we monitored [^{3}H]gabapentin binding to membranes and lipid raft fractions from both the cerebellum and the $\alpha_2\delta$-2 cell line. In the cerebellum, we found that the apparent K_D decreased 4.8-fold from 385 nM in membranes to 80 nM in lipid rafts. In the tsA-201 cell line, we found that the apparent K_D decreased ninefold from 474 to 53 nM. A reduction in K_D of up to 10-fold has been observed previously after purification or dialysis of native $\alpha_2\delta$-1. This was attributed to the loss of an unknown endogenous ligand (Dissanayake et al., 1997; Brown et al., 1998). Given that we find most $\alpha_2\delta$-2 to be present in lipid rafts, the increased affinity for gabapentin when $\alpha_2\delta$-2 is isolated in the lipid raft fraction may therefore be a result of the disruption of interaction of $\alpha_2\delta$-2 with a soluble endogenous ligand or one that has been solubilized by Triton X-100, with which gabapentin normally competes for binding.

Effect of a mutation in $\alpha_2\delta$-2 that abrogates gabapentin binding

We then made a mutation R282 in $\alpha_2\delta$-2, because an equivalent mutation in $\alpha_2\delta$-1 was found to prevent gabapentin binding to $\alpha_2\delta$-1 (Wang et al., 1999). In agreement with this, the R282A mutant $\alpha_2\delta$-2 showed a marked reduction in affinity for gabapentin, and the affinity of the R282A mutant $\alpha_2\delta$-2 for [^{3}H]gabapentin was not enhanced in the cholesterol-rich microdomain fraction. It is therefore likely that, if gabapentin binds at the same site as an endogenous ligand, to an exofacial binding site on $\alpha_2\delta$-2, and if the apparent affinity for gabapentin is enhanced in the cholesterol-rich microdomain fraction because of loss of interaction with this endogenous ligand, then R282A $\alpha_2\delta$-2 does not bind the endogenous ligand. It was therefore of interest to determine whether binding of this unknown endogenous ligand is relevant to the functionality of $\alpha_2\delta$-2. Comparison of the effect of wild-type $\alpha_2\delta$-2 and R282A $\alpha_2\delta$-2 on calcium channel currents showed this mutation to significantly reduce the functionality of $\alpha_2\delta$-2 by ~33%. This finding suggests that, if there is an endogenous ligand associated with $\alpha_2\delta$-2, as predicted for $\alpha_2\delta$-1, that normally binds in the same site as gabapentin (Dissanayake et al., 1997; Brown et al., 1998), this might be essential for its full functionality or for the stability of the protein.

Conclusion

The identification here of $\alpha_2\delta$-2 as a lipid raft protein opened the question as to whether this subunit associates with particular proteins in these cholesterol-rich microdomains and also whether it has other signaling roles. We identified that the properties of $\alpha_2\delta$-2 are altered in the lipid raft fraction, as evidenced by the increased affinity for [^{3}H]gabapentin. We identified $Ca_V2.1$ to be strongly concentrated with $\alpha_2\delta$-2 in lipid rafts from both cerebellum and after heterologous expression and have shown that cholesterol depletion enhances $Ca_V2.1/\alpha_2\delta$-2/β4 currents. We also identified that lipid raft proteins of the SPFH family coimmunoprecipitate with $\alpha_2\delta$-2. These proteins are submembrane scaffold proteins that interact with several types of signaling complex (Langhorst et al., 2005). In the future, we will examine whether they play a role in anchoring the calcium channel proteins in these microdomains or in regulating their endocytosis.

References

Barclay J, Rees M (2000) Genomic organization of the mouse and human $\alpha2\delta2$ voltage-dependent calcium channel subunit genes. Mamm Genome 11:1142–1144.

Barclay J, Balaguero N, Mione M, Ackerman SL, Letts VA, Brodbeck J, Canti C, Meir A, Page KM, Kusumi K, PerezReyes E, Lander ES, Frankel WN, Gardiner RM, Dolphin AC, Rees M (2001) Ducky mouse phenotype of epilepsy and ataxia is associated with mutations in the *Cacna2d2* gene and decreased calcium channel current in cerebellar Purkinje cells. J Neurosci 21:6095–6104.

Brodbeck J, Davies A, Courtney J-M, Meir A, Balaguero N, Canti C, Moss FJ, Page KM, Pratt WS, Hunt SP, Barclay J, Rees M, Dolphin AC (2002) The ducky mutation in *Cacna2d2* results in altered Purkinje cell morphology and is associated with the expression of a truncated $\alpha_2\delta$-2 protein with abnormal function. J Biol Chem 277:7684–7693.

Brown JP, Dissanayake VU, Briggs AR, Milic MR, Gee NS (1998) Isolation of the [^{3}H]gabapentin-binding protein/alpha 2 delta Ca^{2+} channel subunit from porcine brain: development of a radioligand binding assay for alpha 2 delta subunits using [^{3}H]leucine. Anal Biochem 255:236–243.

Burgess DL, Gefrides LA, Foreman PJ, Noebels JL (2001) A cluster of three novel Ca^{2+} channel gamma subunit genes on chromosome 19q13.43: evolution and expression profile of the gamma subunit gene family. Genomics 71:339–350.

Campbell V, Berrow NS, Fitzgerald EM, Brickley K, Dolphin AC (1995) Inhibition of the interaction of G protein G_o with calcium channels by the calcium channel β-subunit in rat neurones. J Physiol (Lond) 485:365–372.

Canti C, Davies A, Dolphin AC (2003) Calcium channel $\alpha_2\delta$ subunits: structure, functions and target site for drugs. Curr Neuropharmacol 1:209–217.

Canti C, Nieto-Rostro M, Foucault I, Heblich F, Wratten J, Richards MW, Hendrich J, Douglas L, Page KM, Davies A, Dolphin AC (2005) The metal-ion-dependent adhesion site in the Von Willebrand factor-A domain of $\alpha2\delta$ subunits is key to trafficking voltage-gated Ca^{2+} channels. Proc Natl Acad Sci USA 102:11230–11235.

Catterall WA (2000) Structure and regulation of voltage-gated Ca^{2+} channels. Annu Rev Cell Dev Biol 16:521–555.

Chalfie M, Au M (1989) Genetic control of differentiation of the *Caenorhabditis elegans* touch receptor neurons. Science 243:1027–1033.

Christian AE, Haynes MP, Phillips MC, Rothblat GH (1997) Use of cyclodextrins for manipulating cellular cholesterol content. J Lipid Res 38:2264–2272.

Cole RL, Lechner SM, Williams ME, Prodanovich P, Bleicher L, Varney MA, Gu G (2005) Differential distribution of voltage-gated calcium channel $\alpha_2\delta$ (alpha2delta) subunit mRNA-containing cells in the rat central nervous system and the dorsal root ganglia. J Comp Neurol 491:246–269.

De Jongh KS, Warner C, Catterall WA (1990) Subunits of purified calcium channels. $\alpha2$ and δ are encoded by the same gene. J Biol Chem 265:14738–14741.

Dissanayake VUK, Gee NS, Brown JP, Woodruff GN (1997) Spermine modulation of specific [^{3}H]-gabapentin binding to the detergent-solubilized porcine cerebral cortex $\alpha_2\delta$ calcium channel subunit. Br J Pharmacol 120:833–840.

Ellis SB, Williams ME, Ways NR, Brenner R, Sharp AH, Leung AT, Campbell KP, McKenna E, Koch WJ, Hui A, Schwartz A, Harpold MM (1988) Sequence and expression of mRNAs encoding the α_1 and α_2 subunits of a DHP-sensitive calcium channel. Science 241:1661–1664.

Ertel EA, Campbell KP, Harpold MM, Hofmann F, Mori Y, Perez-Reyes E, Schwartz A, Snutch TP, Tanabe T, Birnbaumer L, Tsien RW, Catterall WA (2000) Nomenclature of voltage-gated calcium channels. Neuron 25:533–535.

Fagan KA, Smith KE, Cooper DM (2000) Regulation of the Ca^{2+}-inhibitable adenylyl cyclase type VI by capacitative Ca^{2+} entry requires localization in cholesterol-rich domains. J Biol Chem 275:26530–26537.

Felix R, Gurnett CA, De Waard M, Campbell KP (1997) Dissection of functional domains of the voltage-dependent Ca^{2+} channel $\alpha2\delta$ subunit. J Neurosci 17:6884–6891.

Foster LJ, De Hoog CL, Mann M (2003) Unbiased quantitative proteomics of lipid rafts reveals high specificity for signaling factors. Proc Natl Acad Sci USA 100:5813–5818.

Glebov OO, Bright NA, Nichols BJ (2006) Flotillin-1 defines a clathrin-independent endocytic pathway in mammalian cells. Nat Cell Biol 8:46–54.

Gong HC, Hang J, Kohler W, Li L, Su TZ (2001) Tissue-specific expression and gabapentin-binding properties of calcium channel $\alpha_2\delta$ subunit subtypes. J Membr Biol 184:35–43.

Goodman MB, Ernstrom GG, Chelur DS, O'Hagan R, Yao CA, Chalfie M (2002) MEC-2 regulates *C. elegans* DEG/ENaC channels needed for mechanosensation. Nature 415:1039–1042.

Gurnett CA, De Waard M, Campbell KP (1996) Dual function of the voltage-dependent Ca^{2+} channel $\alpha_2\delta$ subunit in current stimulation and subunit interaction. Neuron 16:431–440.

Hans M, Urrutia A, Deal C, Brust PF, Stauderman K, Ellis SB, Harpold MM, Johnson EC, Williams ME (1999) Structural elements in domain IV that influence biophysical and pharmacological properties of human α_{1A}-containing high-voltage-activated calcium channels. Biophys J 76:1384–1400.

Hobom M, Dai S, Marais E, Lacinova L, Hofmann F, Klugbauer N (2000) Neuronal distribution and functional characterization of the calcium channel $\alpha_2\delta$-2 subunit. Eur J Neurosci 12:1217–1226.

Jay SD, Sharp AH, Kahl SD, Vedvick TS, Harpold MM, Campbell KP (1991) Structural characterization of the dihydropyridine-sensitive calcium channel α_2-subunit and the associated δ peptides. J Biol Chem 266:3287–3293.

Klugbauer N, Lacinova L, Marais E, Hobom M, Hofmann F (1999) Molec-

ular diversity of the calcium channel $\alpha2$-δ subunit. J Neurosci 19:684–691.

Klugbauer N, Marais E, Hofmann F (2003) Calcium channel alpha2delta subunits: differential expression, function, and drug binding. J Bioenerg Biomembr 35:639–647.

Langhorst MF, Reuter A, Stuermer CA (2005) Scaffolding microdomains and beyond: the function of reggie/flotillin proteins. Cell Mol Life Sci 62:2228–2240.

Marais E, Klugbauer N, Hofmann F (2001) Calcium channel alpha(2)delta subunits: structure and gabapentin binding. Mol Pharmacol 59:1243–1248.

Mori Y, Friedrich T, Kim M-S, Mikami A, Nakai J, Ruth P, Bosse E, Hofmann F, Flockerzi V, Furuichi T, Mikoshiba K, Imoto K, Tanabe T, Numa S (1991) Primary structure and functional expression from complementary DNA of a brain calcium channel. Nature 350:398–402.

Morrow IC, Parton RG (2005) Flotillins and the PHB domain protein family: rafts, worms and anaesthetics. Traffic 6:725–740.

Moss FJ, Viard P, Davies A, Bertaso F, Page KM, Graham A, Canti C, Plumpton M, Plumpton C, Clare JJ, Dolphin AC (2002) The novel product of a five-exon *stargazin*-related gene abolishes $Ca_V2.2$ calcium channel expression. EMBO J 21:1514–1523.

Owczarek CM, Treutlein HR, Portbury KJ, Gulluyan LM, Kola I, Hertzog PJ (2001) A novel member of the STOMATIN/EPB72/mec-2 family, stomatin-like 2 (STOML2), is ubiquitously expressed and localizes to HSA chromosome 9p13.1. Cytogenet Cell Genet 92:196–203.

Page KM, Heblich F, Davies A, Butcher AJ, Leroy J, Bertaso F, Pratt WS, Dolphin AC (2004) Dominant-negative calcium channel suppression by truncated constructs involves a kinase implicated in the unfolded protein response. J Neurosci 24:5400–5409.

Price MP, Thompson RJ, Eshcol JO, Wemmie JA, Benson CJ (2004) Stomatin modulates gating of acid-sensing ion channels. J Biol Chem 279:53886–53891.

Rivera-Milla E, Stuermer CA, Malaga-Trillo E (2006) Ancient origin of reggie (flotillin), reggie-like, and other lipid-raft proteins: convergent evolution of the SPFH domain. Cell Mol Life Sci 63:343–357.

Sakurai T, Hell JW, Woppmann A, Miljanich GP, Catterall WA (1995) Immunochemical identification and differential phosphorylation of alternatively spliced forms of the α_{1A} subunit of brain calcium channels. J Biol Chem 270:21234–21242.

Sakurai T, Westenbroek RE, Rettig J, Hell J, Catterall WA (1996) Biochemical properties and subcellular distribution of the BI and rbA isoforms of α_{1A} subunits of brain calcium channels. J Cell Biol 134:511–528.

Scherer PE, Okamoto T, Chun M, Nishimoto I, Lodish HF, Lisanti MP (1996) Identification, sequence, and expression of caveolin-2 defines a caveolin gene family. Proc Natl Acad Sci USA 93:131–135.

Shistik E, Ivanina T, Puri T, Hosey M, Dascal N (1995) Ca^{2+} current enhancement by $\alpha2/\delta$ and β subunits in *Xenopus* oocytes: contribution of changes in channel gating and $\alpha1$ protein level. J Physiol (Lond) 489:55–62.

Sutton KG, Snutch TP (2001) Gabapentin: a novel analgesic targeting voltage-gated calcium channels. Drug Dev Res 54:167–172.

Sutton KG, Martin DJ, Pinnock RD, Lee K, Scott RH (2002) Gabapentin inhibits high-threshold calcium channel currents in cultured rat dorsal root ganglion neurones. Br J Pharmacol 135:257–265.

Taverna E, Saba E, Rowe J, Francolini M, Clementi F, Rosa P (2004) Role of lipid microdomains in P/Q-type calcium channel (Cav2.1) clustering and function in presynaptic membranes. J Biol Chem 279:5127–5134.

Taylor CP (2004) The biology and pharmacology of calcium channel alpha2-delta proteins Pfizer Satellite Symposium to the 2003 Society for Neuroscience Meeting. Sheraton New Orleans Hotel, New Orleans, LA November 10, 2003. CNS Drug Rev 10:183–188.

Toselli M, Biella G, Taglietti V, Cazzaniga E, Parenti M (2005) Caveolin-1 expression and membrane cholesterol content modulate N-type calcium channel activity in NG108–15 cells. Biophys J 89:2443–2457.

van Hooft JA, Dougherty JJ, Endeman D, Nichols RA, Wadman WJ (2002) Gabapentin inhibits presynaptic Ca^{2+} influx and synaptic transmission in rat hippocampus and neocortex. Eur J Pharmacol 449:221–228.

Vega-Hernandez A, Felix R (2002) Down-regulation of N-type voltage-activated Ca^{2+} channels by gabapentin. Cell Mol Neurobiol 22:185–190.

Walker D, De Waard M (1998) Subunit interaction sites in voltage-dependent Ca^{2+} channels. Trends Neurosci 21:148–154.

Wang MH, Offord J, Oxender DL, Su TZ (1999) Structural requirement of the calcium-channel subunit $\alpha_2\delta$ for gabapentin binding. Biochem J 342:313–320.

Whittaker CA, Hynes RO (2002) Distribution and evolution of von Willebrand/integrin A domains: widely dispersed domains with roles in cell adhesion and elsewhere. Mol Biol Cell 13:3369–3387.